Indian Journal of Pure & Applied Physics
Vol. 62, October 2024, pp. 875-883
DOI: 10.56042/ijpap.v62i10.11987

Carbon derived from Jute Sacks For Low-Cost and Efficient Counter Electrodes of Dye-Sensitized Solar Cells

Khom Narayan Chaudhary[a], Sanjay Rimal[a], Mohan Prasad Sapkota[a], Anupam K C[b], Umesh Lawaju[a], Mim Lal Nakarmi[c], Manoj Pandey[d] & Prakash Joshi[e*]

[a]Department of Physics, Patan Multiple Campus, Tribhuvan University 44700, Nepal

[b]Materials Science, Engineering and Commercialization Program (MSEC), Texas State University, San Marcos TX 78666, USA

[c]Department of Physics, Brooklyn College and the Graduate Center of the City University of New York, Brooklyn, NY 11210, USA

[d]Department of Physics, Kathmandu University, 45200, Nepal

[e]Department of Physics, Bhaktapur Multiple Campus, Tribhuvan University 44800 Nepal

Received 22 June 2024; accepted 12 September 2024

Non-activated and activated carbons derived from jute sacks were used as counter electrode (CE) materials of dye-sensitized solar cells (DSSCs). The non-activated carbon sample was synthesized by carbonization of jute fibers at 600°C in N_2. The activated carbon samples were synthesized by carbonizing the $ZnCl_2$ activated jute at 600 and 800°C in N_2. The x-ray diffraction revealed that the jute-based carbon samples comprised of graphitic and amorphous carbons. Raman spectroscopy disclosed that the disordered carbon was dominant in all samples. Based on the energy dispersive x-rays spectroscopy measurements, activated carbon prepared at 800 °C had the highest amount of carbon content (~94.3%). The surface textural properties of the samples were investigated with N_2 adsorption-desorption experiment. Brunauer-Emmett-Teller surface area of non-activated (NACJ6), activated at 600 °C (ACJ6) and activated at 800 °C (ACJ8) carbon samples were 23.73, 1912, and 1613 m^2g^{-1}, respectively, and their corresponding pore volumes were 0.02448, 1.114 and 0.9625 cm^3g^{-1}, respectively. ACJ8 with the highest carbon content, moderately high surface area, and micropores and mesopores/macropores demonstrated superior catalytic ability among the samples. The efficiency of the light to electric power conversion of the DSSCs using ACJ8, ACJ6, and NACJ6 as CEs were found to be about 3.35, 2.75, and 0.88%, respectively, compared to 3.39% that of the DSSC using platinum (Pt). Obtained efficiency comparable to Pt based DSSC using the ACJ8 sample implies that the jute-based activated carbon can be an inexpensive and efficient CE material alternative to Pt for commercialization.

Keywords: Activated carbon; Counter electrode; Catalyst; DSSCs; Iodide/tri-iodide ions; Jute; Platinum

1 Introduction

Dye-sensitized solar cells (DSSCs) are considered as cost-effective alternative devices to conventional solar cells[1]. A DSSC is an assembly of photoelectrode and counter electrode (CE) with an electrolyte encapsulated between the electrodes. The photoelectrode is the front electrode, typically consists of a fluorine doped tin oxide (FTO)-glass substrate coated with a film of high band gap mesoporous nanoparticles such as titanium dioxide (TiO_2). A monolayer of a dye molecules is adsorbed on the TiO_2. The dye molecules inject their electrons into TiO_2 film as they receive sunlight. The photoelectrons diffuse in the TiO_2 film and move to the CE via an external circuit. Generally, a CE is an FTO-glass substrate coated with a catalyst like platinum (Pt).The dye molecules are regenerated by receiving electrons from iodide ions in the electrolyte. After donating electrons, iodide ions become tri-iodide ions which migrate toward the CE. The tri-iodide ions receive electrons at the CE and turns to iodide ions. The Pt coated on the CE enhances the conversion of tri-iodide into iodide ions[1–11]. However, high price of Pt motivated researchers to develop low-cost alternate materials for CEs. Carbonaceous materials like activated carbon[8,12–18], carbon black[1,19,20], carbon nanotubes[21–23], carbon nanofibers[5,7,24], graphene[25,26], and lampblack[9–11] have been employed as CE materials alternative to Pt.

Among the carbonaceous materials, the activated carbon is promising because of their high surface area and porosity[14]. Additionally, activated carbons can be synthesized from readily available various types of biomasses using simple method[27–31]. Thus, biomass-

*Corresponding author: (E-mail: prakash.joshi@bkmc.tu.edu.np)

based activated carbon can be a low-cost CE material for DSSCs. Catalytic ability of a carbonaceous material is affected by its surface textural properties like surface area[14], porosity and pore size distribution[32]. Also, the purity of CE material may be another influential factor. Surface textural properties and structural composition of the biomass-based carbon are greatly influenced by activation process and carbonization temperature[27–29,31]. In this report, we prepared activated carbons from jute sacks, and employed them as CE material for DSSCs. Generally, jute sacks are used for packing commodities and used jute sacks are disposed as a waste. We have utilized waste sacks as it is readily available and hence a low-cost precursor for the preparation of the carbonaceous catalyst. Three different types of carbon samples: non-activated, activated at 600 °C and activated at 800 °C were derived from the jute sacks, and characterized for their surface texture, porosity, structural and chemical composition properties to study the influence of the activation conditions. The carbon samples were used as counter electrode (CE) materials of dye-sensitized solar cells (DSSCs) to study their catalytic ability and found that the solar cell with the activated carbon carbonized at 800 °C exhibited superior photovoltaic performance with the efficiency comparable to the efficiency of the reference solar cell using Pt.

2 Experimental Method

2.1 Preparation of Non-Activated and Activated Carbons

Slices of used jute sacks were boiled in distilled water with detergent and jute fibers were extracted from them. The jute fibers were used as precursors for the preparation of carbons. The method of preparation of the carbons is similar to that described elsewhere[27,28,31]. The non-activated carbon was prepared by heating the precursor in a quartz tube furnace (Zhengzhou Protech Technology Co., LTD, China) at 600 °C in N_2 for 4 hours. To prepare the activated carbon samples, the jute fibers were soaked in aqueous solution of $ZnCl_2$ for 24 hours. Equal amounts of jute fibers and $ZnCl_2$ by weight were taken for the activation process. The activated jute fibers were dried and carbonized at two different temperatures at 600 and 800 °C in N_2. The carbon samples were washed with dilute HCl and distilled water successively. Then the samples were dried, ground, and filtered (through 120-micron sieve). The non-activated carbon carbonized at 600 °C, the activated carbon carbonized at 600 °C, and the activated carbon carbonized at 800 °C, were labelled as NACJ6, ACJ6, and ACJ8, respectively.

2.2 Characterization of Carbon Samples

The X-ray diffraction (XRD) measurements of the samples were conducted for structural characterization using a Bruker D2 PHASER diffractometer (λ = 1.54 Å). Raman spectroscopy measurements were performed by using Laser of 532 nm wavelength. Scanning electron microscopy (SEM) and energy dispersive X-ray spectroscopy (EDS) were performed using FEI Helios Nanolab 400 Scanning Electron Microscope.

Surface textural parameters like pore volume and pore size distribution (PSD) of activated carbon (catalyst) influence the transport mechanism of electrolyte[33] and hence its catalytic ability. Surface textural properties of the non-activated and activated carbons were investigated by N_2 adsorption and desorption experiments[34,35] using Autosorb-1C, Quantachrome.

2.3 Fabrication of Dye-Sensitized Solar Cells

DSSCs with CEs coated with NACJ6, ACJ6, and ACJ8 samples were prepared. A DSSC with Pt CE was also prepared as a reference solar cell. The structure of a DSSC with carbon-based CE is shown in Figure 1. The procedure of the preparation of the

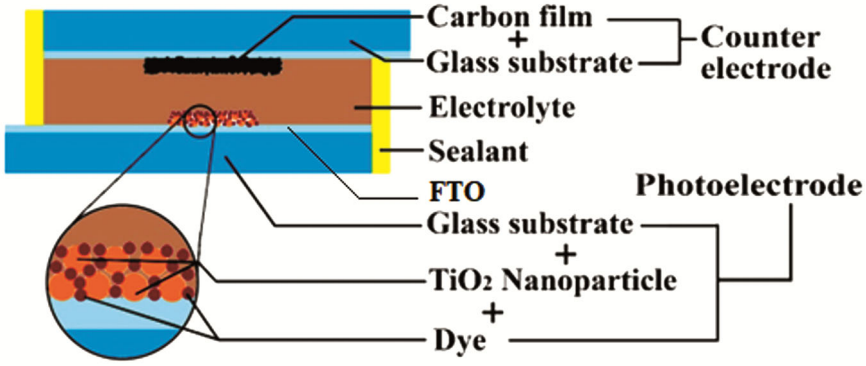

Fig. 1 — Schematic diagram of a cross-section of a DSSC with a carbon-based

carbon-based CEs was similar to the previous reports[5,6]. Carbon paste was prepared by mixing the carbon sample with an aqueous solution of carboxy methylcellulose sodium salt (CMC) of 2% concentration. The CMC was added as a binder. The carbon paste was doctor bladed onto FTO-glass substrates and dried overnight in an oven at 70 °C. Pt based CEs were prepared by coating its precursor (Plati Sol, Solaronix) onto an FTO-glass substrates and then heating the precursor at 450 °C for 45 minutes.

The photoelectrodes of the DSSCs were prepared as follows[8,9]. A thin layer of nano-crystalline TiO_2 paste (TiNanoxide T/SP, Solaronix) was doctor bladed onto FTO-glass substrates. The TiO_2 paste was sintered at 450 °C for 45 minutes and then cooled down to ~80 ºC. The sintered TiO_2 film was soaked in 0.5 mM N-719 dye (Ruthenizer 535-bisTBA, Solaronix) solution for 24 hours. The photoelectrode and counter electrode were assembled with a paraffin film which acts as a sealant and spacer. Electrolyte (Idolyte AN-50, Solaronix) containing iodide and tri-iodide ions was injected into the gap between the electrodes. A DSSC with Pt coated CE was also fabricated as a reference solar cell[9].

2.4 Photovoltaic Characterization of DSSCs

The photovoltaic performance of the DSSCs was characterized with the current density-voltage (J-V) characteristics[6,36] of the solar cells under the illumination of ~100 mW/cm^2 from a solar simulator (Abet technologies, model 11002). Source meter (Ossilla, UK) was employed to obtain the J-V curves. Photovoltaic parameters such as light- to-electricity conversion efficiency (η), short-circuit current density (J_{sc}), open circuit voltage (V_{oc}), fill factor (FF), and series resistance (R_s) of the solar cells were calculated from the J-V curves[6,36]. An application software provided with the source meter (Ossilla) was used to determine the values of the photovoltaic parameters.

3 Results and discussion

3.1 XRD and Raman spectroscopy

Figure 2 shows the XRD patterns of the carbon samples with two broad and characteristic peaks due to reflections from (002) and (100) plans centered around 2θ =24.96° and 43.64° from NACJ6 (Fig. 2(a)), 2θ =25.05°and 43.10° from ACJ6 (Fig. 2(b)), and 2θ =26.57° and 43.69° from ACJ8 (Fig, 2(c)). These broad characteristic peaks indicate the carbon samples contain graphitic crystallites[29,37,38]. Moreover, the XRD patterns of the carbons show large background in the region of (002) peaks[39]. According to previous reports[39,40], such background signal is attributed to the reflection from amorphous carbon. Lu *et al.* [41] attributed that the intensity of (002) peak is the sum of the intensity scattered from crystalline carbon and amorphous carbon[39,41]. Based on the XRD patterns of the activated carbons, the intensity contributed from the amorphous carbon seems to be much higher than that from the crystalline carbon indicating significantly high fraction of amorphous carbon present compared to the crystalline carbon in these samples. Also, the XRD-pattern of ACJ6 (Fig. 2(b)) shows sharp peaks at about 2θ=31.63, 36.44, 47.66, 56.47, 62.68 and 68.09°. The peaks correspond to the reflection from (100), (101), (102), (110), (103), and (112) planes of ZnO[42,43]. Gnawali *et al.*[31], while reporting the preparation of carbon from $ZnCl_2$ activated *Terminalia chebula* seed for super capacitor application, mentioned that the $ZnCl_2$ is partially converted into solid ZnO at higher pyrolysis temperature above 290 °C. The low intensity ZnO peaks seen in the XRD pattern of ACJ6, indicate that ZnO still remained as impurity even after washing the sample with HCl.

Figure 3 shows the Raman spectra of NACJ6, ACJ6 and ACJ8 samples. Raman spectrum of all samples showed two distinct peaks centered at 1347.09 and 1588.60 cm^{-1} for NACJ6, at 1346.38 and 1589.99 cm^{-1} for ACJ6, and at 1345.92 and 1589.49 cm^{-1} for ACJ8 samples. The peak 2 in the samples at 1588.60, 1589.99 and 1589.49 cm^{-1} correspond to the G-band which is omnipresent in all the carbonized samples[28,44]. This indicates the presence of ordered graphitic structure which is attributed to E_{2g} mode vibrations of graphitic planes. Additionally, the peak 1 in the samples at 1347.09,

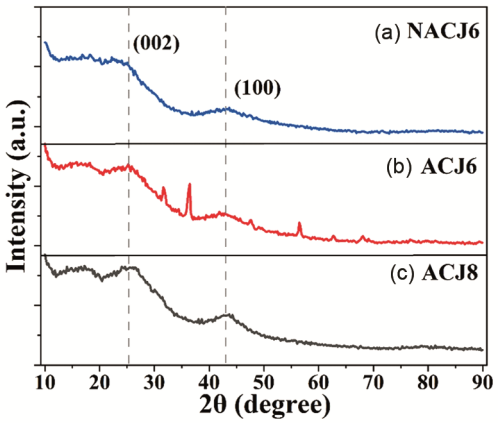

Fig. 2 — XRD pattern of (a) NACJ6, (b) ACJ6, and (c) ACJ8

1346.38, and 1345.92 cm^{-1} correspond to the D-band which indicates the presence of disordered carbon structure[5,28,29,44]. The Raman spectra were fitted with Lorentzian line shapes to calculate the portions of the ordered and disordered carbon phases[45]. The NACJ6 sample contains about 76.94% disordered and 23.05% ordered carbon. Similarly, the ACJ6 sample contains about 75.00% disordered and 24.99% ordered carbon, and the ACJ8 sample contains about 74.36% disordered and 25.63% ordered carbon. This shows that amorphous carbon dominates the crystalline form of the carbon in all samples, however, degree of crystallinity increased slightly as carbonization temperature is increased from 600 to 800 °C. These results of Raman spectroscopy of the carbon samples correlate with their XRD patterns.

3.2 SEM images and EDS

Figure 4 shows the SEM images of the carbon samples. Fig. 4(a-c) are the SEM images of NACJ6, ACJ6, and ACJ8 samples, respectively. The size of the scale bar in each SEM image is 20 µm. The SEM image of NACJ6 shows that the carbon sample consists of irregular shaped particles. Solid cylindrical shaped carbon particles are dominant ones and the size of the particles ranges from few microns to 60 µm. The SEM images of ACJ6 and ACJ8 show that the particles are mostly granular in shape and their sizes are less than 20 µm. It seems that the carbonization of the activated precursors yielded smaller particles compared to the carbonization of the precursor without activation. Generally, smaller particles yield larger surface area.

Figure 5 shows the SEM-EDS spectra of NACJ6, ACJ6, and ACJ8. The scanned area of EDS of each

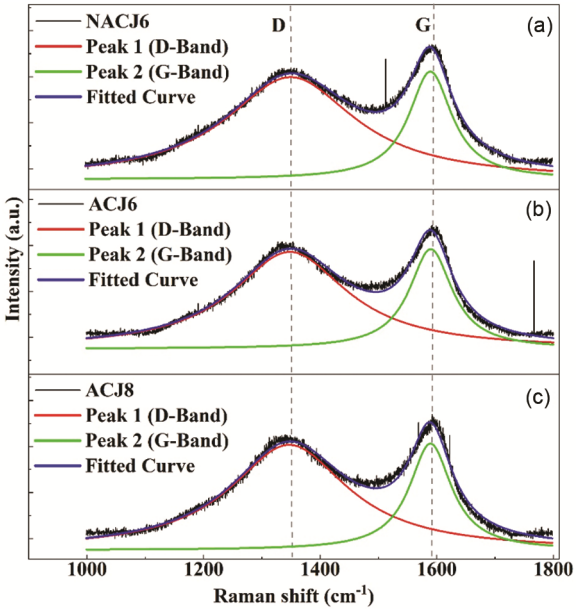

Fig. 3 — Raman spectrum of (a) NACJ6, (b) ACJ6, and (c) ACJ8

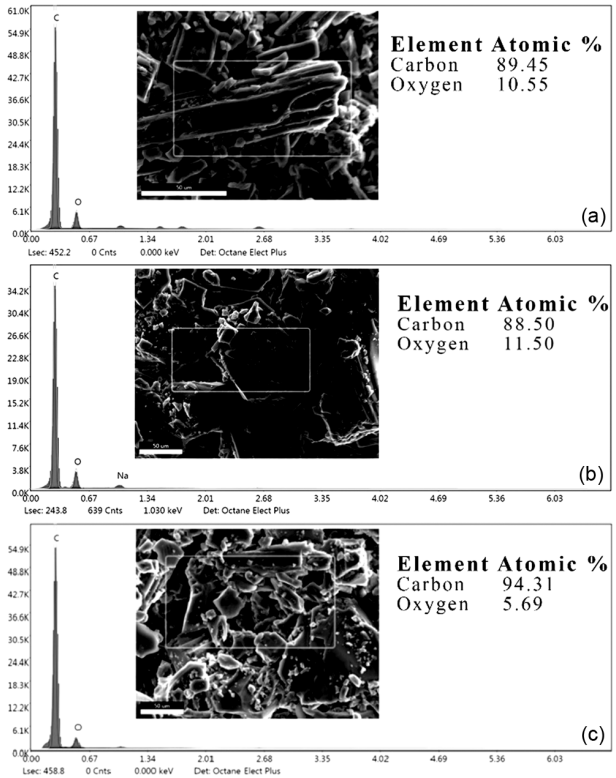

Fig. 5 — EDS spectrum of (a) NACJ6, (b) ACJ6, and (c) ACJ8

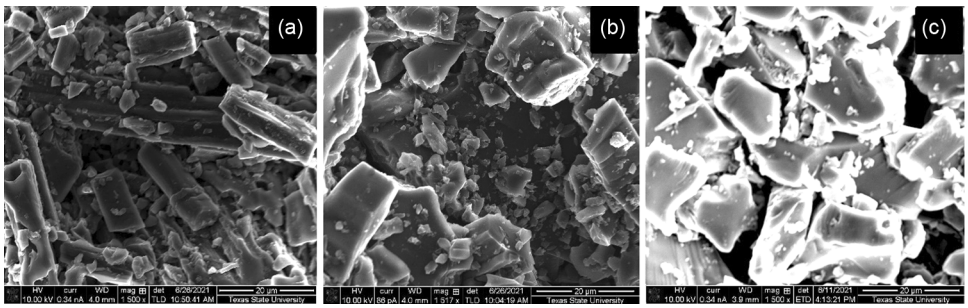

Fig. 4 — SEM image of (a) NACJ6, (b) ACJ6, and (c) ACJ8

sample is enclosed within a square in its SEM image shown in inset. Based on the EDS results, the carbon content in NACJ6, ACJ6, and ACJ8 are about 89.5, 88.5, and 94.3%, (atomic %), respectively. The EDS revealed that carbon content in NACJ6 and ACJ6 are almost equal, but significantly high in ACJ8 which is also consistent with higher integrated intensity of the peaks seen in the XRD pattern of ACJ8 (compared to those of NACJ6 and ACJ6). This indicates that higher carbonization temperature is more favorable for reducing impurities in the biomass derived carbon samples.

3.3 Surface Textural Properties

The N_2 adsorption-desorption isotherms of NACJ6, ACJ6, and ACJ8 are shown in Fig. 6. The N_2 adsorption-desorption isotherms were recorded by varying relative pressure (P/P_o) from ~0.05 to 0.99 at

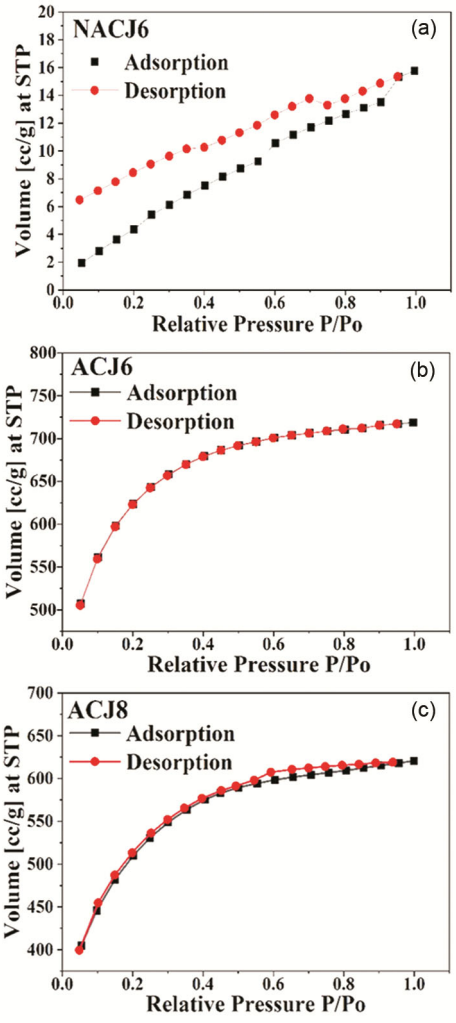

Fig. 6 — N_2 adsorption–desorption isotherm plots for (a) NACJ6, (b) ACJ6, and (c) ACJ8

bath temperature of 77.3 K, where P is pressure of N_2 (adsorptive) and P_o is saturation pressure. The isotherm of NACJ6 shows the adsorption of N_2 increases linearly with increasing P/P_o. The linear section of the isotherm indicates formation of multilayer of N_2 on the surface of the carbon. This isotherm belongs to Type II and it is a characteristic of a non-porous or macroporous solid[34]. Additionally, the isotherm shows that the volume of N_2 adsorbed by this carbon at the entire range of the gas pressure is extremely small implyingits low surface area. In contrast, the isotherms of ACJ6 and ACJ8 are nonlinear. The N_2 adsorption increases steadily above ~0.5 P/P_o and approaches a limiting value at ~0.99 P/P_o. The volume of N_2 adsorbed on carbon surfaces are notably higher at all pressure indicating its surface area is significantly high compared to that of NACJ6. For ACJ6, the isotherm is of Type-I[34,35] and it indicates that ACJ6 is a mostly microporous carbon[34,37]. Pore sizes in materials are categorized into micropores (< 2 nm), mesopores (2 nm <50nm), and macropores (> 50 nm)[34]. In case of ACJ8, its isotherm shows a weak hysteresis loop at ~0.5 to 0.8 P/P_o due to capillary condensation of the adsorbate in mesopores. This isotherm belongs to Type IV and it indicates the formation of significant number of mesopores along with dominant micropores in this carbon[29,34,37]. The isotherm also depicts that adsorption of less amount of N_2 on ACJ8 compared to ACJ6 indicating its smaller specific surface area compared to that of later one.

Figure 7 shows the PSD profiles of NACJ6, ACJ6, and ACJ8 obtained by Density Function Theory (DFT) method[29,33,46]. The PSD profiles reveal that NACJ6 is the least porous whereas ACJ6 and ACJ8 are highly porous. Also, the profiles depict the presence of higher portion of micropores in ACJ6 and mesopore in ACJ8. As the size of iodide/tri-iodide ions in the electrolyte used in DSSCs are of a few angstroms in dimensions[12], the pore sizes in the activated carbons are sufficiently larger for easy movement of the ions through the pores.

The surface textural parameters--BET specific surface area (S_{BET}), total pore volume (V_{tot}), and micropore area (S_{micro})-- obtained from the N_2 adsorption-desorption experiments are as follow. The S_{BET}, V_{tot}, and S_{micro} of NACJ6 are 23.73 m^2g^{-1}, 0.02448 cm^3g^{-1}, and 11.54 m^2g^{-1}, respectively. These parameters of ACJ6 are 1912 m^2g^{-1}, 1.114 cm^3g^{-1}, and 1755 m^2g^{-1}, respectively. Similarly, the corresponding values of the parameters of ACJ8 are1613 m^2g^{-1}, 0.9625 cm^3g^{-1}, and 1443 m^2g^{-1}, respectively.

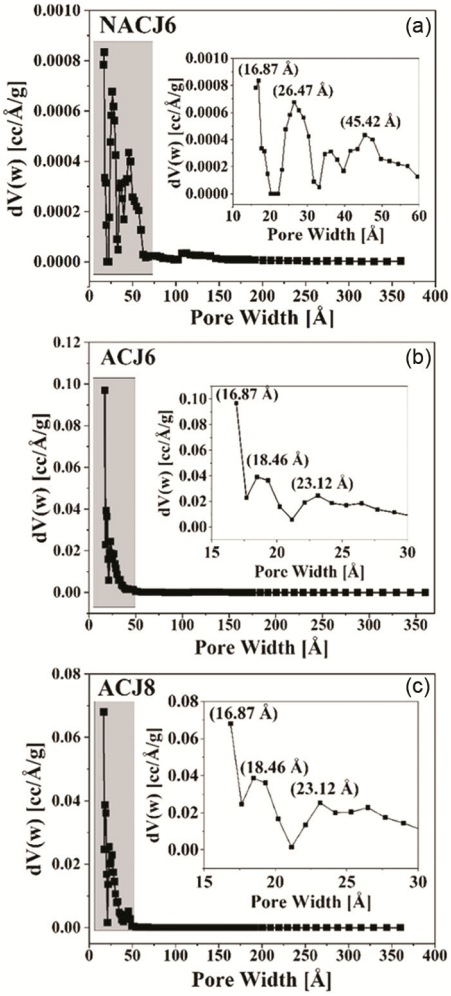

Fig. 7 — Pore size distributions (PSD) obtained from DFT methods for (a) NACJ6, (b) ACJ6, and (c) ACJ8

The specific surface area of the activated carbon samples significantly increased (at least by ~68 times) compared to that of the non-activated carbon because of increase in their porosity. However, the specific surface area of the activated carbon reduced as carbonization temperature was elevated from 600 to 800 °C. This could be due to merge of some of the micropores forming more mesopores during the carbonization at the elevated temperature[29]. The micropore surface area was calculated by t-method (de Boer method)[47]. The cumulative value of mesopore and macropore area (named $S_{meso/macro}$) was calculated by subtracting the micropore area from the total specific surface area (S_{BET}). The $S_{meso/macro}$ of NACJ6, ACJ6, and ACJ8 are 12.19, 157.0, and 170.0 m^2g^{-1}, respectively. The ratio of mesopore/macropore to micropore surface area of ACJ8 is 0.12 and that of ACJ6 is 0.09. Thus, the

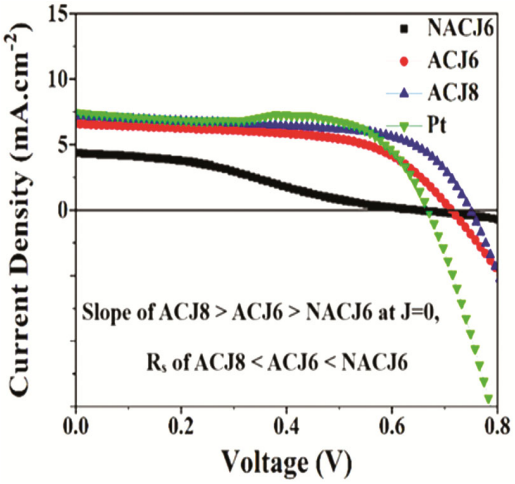

Fig. 8 — J-V Curves of DSSCs with CEs based on NACJ6, ACJ6, ACJ8, and Pt

elevated value of the ratio can be evidence of coalescence of micropores and formation of more mesopores/macropores. These results correlate with the appearance of hysteresis loop in the isotherm and the elevated volume of mesopores seen in the PSD profile of ACJ8.

3.4 Current density-Voltage Characteristics of Dye-Sensitized Solar Cells

Figure 8 shows the J-V curves of the DSSCs with CEs prepared using NACJ6, ACJ6, ACJ8, and Pt. The J-V curves show that the photocurrent from the DSSC with NACJ6 is the lowest and it is notably high from the DSSC with ACJ6. And the solar cell with ACJ8 produced the highest photocurrent which matched to that from the Pt based DSSC. Also, V_{oc} is the largest from the DSSC with ACJ8 while that for the devices with NACJ6 and Pt are nearly equal. Regarding the shape of the J-V curves, the J-V curve of NACJ6 shows least squareness and it improves for ACJ6 and ACJ8, successively. The shapes of J-V curves indicate low FF of the DSSC with NACJ6 and FF improved by notably for the solar cells with ACJ6 and ACJ8. Furthermore, the successive increment of the slope of the J-V curves around J=0 for ACJ6 and ACJ8-based solar cells compared with that of NACJ6 indicates the decreasing trend of R_s of the activated carbon-based solar cells compared with the non-activated carbon-based solar cell. R_s of a solar cell can be estimated from the reciprocal of the slope of the linear part of the J-V curve at J=0[6,48]. The steepness of the J-V curves around J=0 of ACJ6 is significantly large compared with that of NACJ6-based solar cell. And the slope of the J-V curve increases more for ACJ8-

based solar cell and almost matches to that of Pt-based solar cell. This implies that R_s of ACJ8 is the lowest among the carbon-based solar cells and nearly equal to that of the Pt-based solar cell.

The photovoltaic parameters η, J_{sc}, V_{oc}, FF, and R_s of the DSSC with NACJ6 are about 0.88 %, 4.37 $mAcm^{-2}$, 0.64 V, 31.33 %, and 263.46 Ωcm^2, respectively. Those parameters for the solar cells with ACJ6 are about 2.75 %, 6.59 $mAcm^{-2}$, 0.71 V, 58.70 %, and 21.02 Ωcm^2, respectively. Similarly, the values of the parameters for the DSSC with ACJ8 are about 3.35 %, 7.21 $mAcm^{-2}$, 0.74 V, 62.31 %, and 12.77 Ωcm^2, respectively. And the corresponding values of the parameters for the solar cell with Pt are about 3.39 %, 7.45 $mAcm^{-2}$, 0.66 V, 68.15 %, and 10.84 Ωcm^2, respectively. Table 1 lists the photovoltaic parameters of the DSSCs.

The η of the DSSC with ACJ6 is much larger than that of the solar cell with NACJ6. The R_s of NACJ6-based DSSCs is much larger compared to that of ACJ6 solar cell. R_s is a parasitic resistance in a solar cell and it dissipates electric power generated in the solar cell. Thus, higher value of R_s decreased FF[36] and J_{sc}[12] which caused low efficiency of NACJ6 solar cell. This indicates that catalytic ability of the non-activated carbon is significantly poor compared to the activated carbon. The elemental compositions of both of the carbons were similar but the surface area of the activated carbon was significantly larger than that of the non-activated carbon. The higher surface area of the catalyst provides larger catalyst-electrolyte interface for the reduction of tri-iodide ions in the electrolyte. This can be a major cause of superior catalytic ability of the activated carbon to the non-activated carbon. In previous study, Yoon et *al.*[14] adopted activated carbon derived from coconut shells, pine trees, and coals with BET areas of 1,111.32, 963.03, and 754.12 $m^2 g^{-1}$, respectively, as CEs of the DSSCs and reported the efficiencies of 5.90, 6.21, 4.17 % from their respective solar cells compared to 7.20% efficiency from a reference cell with Pt. Their findings indicate carbonaceous CEs with high surface area exhibit better photovoltaic performance but the relation between increase in efficiency of the DSSCs and the surface area of the CE material is not linear one[14].

Similarly, the η of the DSSC with ACJ8 was higher than that of the solar cell with ACJ6. Along with the efficiency, other photovoltaic parameters of ACJ8 were better than those of ACJ6. The EDS and PSD results of ACJ8 and ACJ6 showed that the variation of carbonization temperature results different carbon content and pore size profiles. ACJ8 with high purity provides more catalyst sites at the CE-electrolyte interface which is beneficial for expedite conversion of tri-iodide-ions into iodide ions compared to ACJ6. Regarding the PSDs, micropores were dominant pores in both types of the activated carbons, but the portion of mesopores/macropores was higher in the carbon activated at high temperature. Existence of abundant mesopores/macropores facilitates mass transport of electrolyte through the micropores[28]. This factor could have also enhanced the rate of the reduction of tri-iodide ions in the DSSC with ACJ8. Thus, among all the three types of the carbons based DSSCs, the solar cell with ACJ8 yielded the highest efficiency.

Moreover, the photovoltaic performance of the DSSCs with ACJ8 and Pt were almost same. The J_{sc} and FF of the ACJ8 based DSSC are slightly smaller than that of Pt based because of larger R_s (internal resistance) of the activated carbon-based solar cell compared to that of Pt based solar cell[12]. Smaller values of J_{sc} and FF of the ACJ8 based DSSC could reduce its η significantly compared with that of Pt-based device, however, elevated V_{oc} by about 80 mV of the former device helped to compensate the probable loss of its efficiency and enabled it to yield the efficiency which is comparable to that of Pt based solar cell. Imoto et *al.*[12] also reported the increase in V_{oc} by 60 mV of activated carbon (Bellfine AP-20, commercial activated carbon) based DSSC compared with sputtered Pt based DSSC. The authors attributed such increment of V_{oc} to the positive shift of the formal potential for iodide/tri-iodide ions in the electrolyte. The photovoltaic performance of the DSSCs with ACJ8 and Pt were almost same. The η of DSSC with ACJ8 is very close to that of the Pt-based DSSC. This shows that ACJ8 can be used for commercialization of DSSC with low-cost CE material alternative to Pt.

Table 1 — Photovoltaic parameters of DSSCs with CE based on NACJ6, ACJ6, ACJ8, and Pt

CE	η(%)	$J_{sc}(mAcm^{-2})$	V_{oc}(V)	FF (%)	R_s (Ωcm^2)
NACJ6	0.88	4.37	0.64	31.33	263.46
ACJ6	2.75	6.59	0.71	58.70	21.02
ACJ8	3.35	7.21	0.74	62.31	12.77
Pt	3.39	7.45	0.66	68.15	10.84

4 Conclusion

Activated and non-activated carbon samples were synthesized from jute sacks aiming to employ them as Pt-free low-cost CEs in DSSCs. The carbon samples were characterized by XRD, Raman spectroscopy, SEM, EDS, and N_2 adsorption-desorption experiment for the exploration of their structural properties, chemical composition, and surface textural characteristics. We found the efficiency of the DSSC prepared with the activated carbon has significantly higher efficiency compared to non-activated carbon-based DSSC. Carbon samples activated at 800 °C possessed superior properties with the highest carbon content, moderately high surface area, and micropores and mesopores/macropores and demonstrated superior catalytic ability. The efficiency of the DSSC using the carbon sample activated at 800 °C as CE was found to be close to that obtained from the Pt-based reference DSSC. Hence, the activated carbon can be a novel, low-cost, and efficient CE material alternate to expensive Pt used in dye-sensitized solar cells.

Acknowledgments

This research was funded by University Grants Commission, Nepal (Grant number-MRS-76/77-S&T-63). The authors are also thankful to Associate Prof. Sudarshana Shakya (Bhaktapur Multiple Campus, Tribhuvan University, Nepal), Dr. Bhim Kafle (Kathmandu University), Indian Institute of Technology (IIT), Kanpur, India, and Nepal Academy of Science and Technology (NAST). Also, the authors are thankful to Shared Research Operation (SRO) facility, Texas State University for providing SEM imaging facility.

References

1 Joshi P, Xie Y, Ropp M, Galipeau D, Bailey S & Qiao Q, *Energy Environ Sci*, 2 (2009) 426.
2 O'Regan B & Grätzel M, *Nature*, 353 (1991) 737.
3 Kay A & Grätzel M, *Sol Energy Mater Sol Cells*, 44 (1996) 99.
4 Hauch A & Georg A, *Electrochimica Acta*, 46 (2001) 3457.
5 Joshi P, Zhang L, Chen Q, Galipeau D, Fong H & Qiao Q, *ACS Appl Mater Interfaces*, 2 (2010) 3572.
6 Joshi P, Electrospun Carbon Nanofibers and Composites as Low-Cost Counter Electrodes for Dye-Sensitized Solar Cells, South Dakota State University, (2012).
7 Joshi P, Zhou Z, Poudel P, Thapa A, Wu X-F & Qiao Q, *Nanoscale*, 4 (2012) 5659.
8 Joshi P, *Tribhuvan Univ J*, 32 (2018) 1.
9 Joshi P, Lawaju U & B.k B, *BIBECHANA*, 17 (2020) 58.
10 Lawaju U & Joshi P, *J Nepal Phys Soc*, 8 (2022) 1.
11 Joshi P, Lawaju U K C A, Nakarmi M & Pradhan R, *BIBECHANA*, 20 (2023) 205.
12 Imoto K, Takahashi K, Yamaguchi T, Komura T, Nakamura J & Murata K, *Sol Energy Mater Sol Cells*, 79 (2003) 459.
13 Imoto K, Suzuki M, Takahashi K, Yamaguchi T, Komura T, Nakamura J & Murata K, *Electrochemistry*, 71 (2003) 944.
14 Yoon C H, Chul S K, Ko H H, Yi S & Jeong S H, *J Nanosci Nanotechnol*, 13 (2013) 7875.
15 Joshi P, *Int J Eng Adv Res Tech*, 3 (2017) 8.
16 Buchlová T, Hatala M, Veteška P, Ház A, Novák P, Mackuľak T, Mikula M & Gemeiner P, *Mater Sci Semicond Process*, 171 (2024) 108016.
17 Kanjana N, Maiaugree W, Wechprasit T, Kaewprajak A, Kumnorkaew P, Wongjom P & Infahsaeng Y, *Heliyon*, 10 (2024).
18 Weerasinghe M I U, Kumarage P M L, Amarathunga I G K D, Bandara T M W J, Velauthapillai D, Karunarathne B C, Punniamoorthy R, Rajapakse R M G & Kumara G R A, *J Sci: Adv Mater Dev*, 9 (2024) 100749.
19 Murakami T N, Ito S, Wang Q, Nazeeruddin M K, Bessho T, Cesar I, Liska P, Humphry-Baker R, Comte P, Péchy P & Grätzel M, *J Electrochem Soc*, 153 (2006) A2255.
20 Ramasamy E, Lee W J, Lee D Y & Song J S, *Appl Phys Lett*, 90 (2007) 173103.
21 Suzuki K, Yamaguchi M, Kumagai M & Yanagida S, *Chem Lett*, 32 (2003) 28.
22 Lee W J, Ramasamy E, Lee D Y & Song J S, *ACS Appl Mater Interfaces*, 1 (2009) 1145.
23 Krishnapriya R, Nizamudeen C & Mourad A-H I, *Mater Renew Sustain Energy*, 12 (2023) 257.
24 Zambrzycki M, Piech R, Raga S R, Lira-Cantu M & Fraczek-Szczypta A, *Carbon*, 203 (2023) 97.
25 Wang H & Hu Y H, *Energy Environ Sci*, 5 (2012) 8182.
26 Bayram O, Igman E, Guney H, Demir Z, Yurtcan M T, Cirak C, Hasar U C & Simsek O, *J Mater Sci: Mater Electron*, 31 (2020) 10288.
27 Rajbhandari R, Preparation and Characterization of Activated Carbon from Lapsi (Choerospondias Axillaris) Seed Stone for the Removal of Arsenic (III) from Water, , Tribhuvan University, 2015.
28 Shrestha L K, Shrestha R G, Maji S, Pokharel B P, Rajbhandari R, Shrestha R L, Pradhananga R R, Hill J P & Ariga K, *Nanomaterials*, 10 (2020) 728.
29 Shrestha L K, Shahi S, Gnawali C L, Adhikari M P, Rajbhandari R, Pokharel B P, Ma R, Shrestha R G & Ariga K, *Materials*, 15 (2022) 8335.
30 Shrestha D, *Mater Sci Energy Technol*, 5 (2022) 353.
31 Gnawali C L, Shrestha L K, Hill J P, Ma R, Ariga K, Adhikari M P, Rajbhandari R & Pokharel B P, *J Carbon Res*, 9 (2023) 109.
32 Fang B, Fan S-Q, Kim J H, Kim M-S, Kim M, Chaudhari N K, Ko J & Yu J-S, *Langmuir*, 26 (2010) 11238.
33 Lastoskie C, Gubbins K E & Quirke N, *J Phys Chem*, 97 (1993) 4786.
34 Sing K S W, *Pure Appl Chem*, 57 (1985) 603.
35 Thommes M & Cychosz K A, *Adsorption*, 20 (2014) 233.
36 Nelson J, The Physics of Solar Cells, Imperial College Press, London, (2007) 6.
37 Adan-Mas A, Alcaraz L, Arévalo-Cid P, López-Gómez Félix A & Montemor F, *Waste Management*, 120 (2021) 280.
38 Lee S-M, Lee S-H & Roh J-S, *Crystals*, 11 (2021) 153.
39 Kang D-S, Lee S-M, Lee S-H & Roh J-S, *Carbon Lett*, 27 (2018) 108.

40 Franklin R E, *Acta Cryst*, 3 (1950) 107.
41 Lu L, Sahajwalla V, Kong C & Harris D, *Carbon*, 39 (2001) 1821.
42 Jayachandiran J, Raja A, Arivanandhan M, Jayavel R & Nedumaran D, *J Mater Sci: Mater Electron*, 29 (2018) 3074.
43 Abdessemed A, Rasalingam S, Abdessemed S, Djebbar K E Z & Koodali R, *Int J Photoenergy*, 2019 (2019) 4714107.
44 Tuinstra F & Koenig J L, *The J ChemPhys*, 53 (1970) 1126.
45 K.C. A, Anderson J, Ayala A, Engdahl C, Piner E L & Holtz M W, *J Crystal Growth*, 610 (2023) 127172.
46 Seaton N A, Walton J P R B & Quirke N, *Carbon*, 27 (1989) 853.
47 de Boer J H, Lippens B C, Linsen B G, Broekhoff J C P, van den Heuvel A & Osinga T J, *J Colloid Interf Sci*, 21 (1966) 405.
48 Schroder D K, Semiconductor Material and Device Characterization (John Wiley & Sons), 3rd Edn, (2005) 194.